

Auxiliary particle theory of threshold singularities in photoemission and X-ray absorption spectra: test of a conserving T -matrix approximation

Thomas Schauerte, Johann Kroha and Peter Wölfle

Institut für Theorie der Kondensierten Materie, Universität Karlsruhe, Postfach 6980, 76128 Karlsruhe, Germany
(November 30, 1999)

We calculate the exponents of the threshold singularities in the photoemission spectrum of a deep core hole and its X-ray absorption spectrum in the framework of a systematic many-body theory of slave bosons and pseudofermions (for the empty and occupied core level). In this representation, photoemission and X-ray absorption can be understood on the same footing; no distinction between orthogonality catastrophe and excitonic effects is necessary. We apply the conserving slave particle T -matrix approximation (CTMA), recently developed to describe both Fermi and non-Fermi liquid behavior systems with strong local correlations, to the X-ray problem as a test case. The numerical results for both photoemission and X-ray absorption are found to be in agreement with the exact infrared powerlaw behavior in the weak as well as in the strong coupling regions. We point out a close relation of the CTMA with the parquet equation approach of Nozières *et al.*

PACS numbers: 71.27.+a, 71.10.-w, 75.20.Hr

I. INTRODUCTION

The core level spectral function $A_d(\epsilon)$ of a localized core orbital immersed in a conduction electron sea, as observed in the photoemission of electrons after X-ray absorption has long been known to show nonanalytic threshold behavior characterized by fractional power laws $A_d(\epsilon) \propto \epsilon^{-\alpha_d}$ in the frequency distance to the threshold $\epsilon = \omega - E_0$. As shown by Anderson¹, this can be understood by considering that the sudden creation of a deep hole in the electronic core of an ion in a metal (or the filling of an empty core state) disturbs the Fermi sea of the conduction electrons so strongly that the subsequent relaxation into the new ground state follows a fractional power law in time rather than the usual exponential dependence. This is due to the fact that the ground states of the initial state and the final state are orthogonal in the limit of an infinite system (“orthogonality catastrophe”). At finite, but small ϵ the relaxation process involves excitation of a large number of particle-hole pairs out of the Fermi sea of conduction electrons. A similar situation arises at the X-ray absorption threshold. There it has been argued that in addition to the above an excitonic effect appears, as first discussed by Mahan². A theoretical description requires the use of infinite order perturbation theory.

The problem is in some sense the simplest situation in which strong electron correlations are generated by a sudden change of electron occupations of a level coupled to a Fermi sea. The same generic problem is at the heart of the Kondo problem, or generally speaking, of quantum impurity problems, which can be understood as a succession of X-ray edge problems generated by successive flips of the impurity spin or pseudospin. In an even more general context, such problems arise in lattice models of correlated electrons, when the hopping of an electron from one site to the next changes the occupation of these sites, causing a corresponding rearrangement of

the whole Fermi system. Given the existing evidence that high temperature superconductors, heavy fermion compounds and other metallic systems are governed by strong electron correlation effects, which are at present only poorly understood, there is an urgent need for generally applicable theoretical methods capable of dealing with these complex situations.

A powerful method of many-body physics, which directly addresses the consequences of a change in occupation number of a local level is the pseudoparticle representation^{3,4}. Within this framework one introduces pseudoparticles for each of the states of occupation of a given energy level, i.e. fermions for the singly occupied level and bosons for the empty level. It is well known that a representation of this type for the infinite U Anderson model of a magnetic impurity in a metal can give surprisingly good results already in second-order self-consistent perturbation theory [“non-crossing-approximation” (NCA)] in the hybridization of local level and conduction band⁵. However, at low temperatures and low energies the NCA fails to control the infrared singular behavior of the pseudoparticle spectral functions at threshold. Application of the NCA to the problem of the core hole spectral function gives a threshold exponent α_d independent of the occupation of the core state, in contradiction with the exactly known result.

We have recently developed an approximation scheme, which appears to overcome the difficulties of NCA^{6,7}. It is based on the idea of including singular behavior emerging in any of the two-particle channels. There are two relevant channels, the pseudofermion-conduction electron and the slave boson-conduction electron channel. In both channels the ladder diagrams are summed, the resulting T -matrices are self-consistently included in the self-energies, as is required within a conserving approximation scheme. The main results of this conserving T -matrix approximation (CTMA) are: (i) the (exactly known) infrared threshold exponents of the pseudopar-

ticle spectral functions are recovered⁶, (ii) the thermodynamic quantities spin susceptibility and specific heat show local Fermi liquid behavior in the single channel case⁸ and (iii) in the multi channel case, non-Fermi liquid behavior is found⁸, in quantitative agreement with exact results available in certain limiting cases.

One of the most stringent tests of a many-body method is the calculation of the core hole spectral function. In this paper we report the results of an application of the CTMA to this problem.

The organization of the paper is as follows. In section II, we summarize the most important results of the exact solution of the X-ray model^{9,10}, notably those for the threshold exponents for the photoemission and the X-ray absorption. Then, in section III, we recall the pseudoparticle representation of a spinless Anderson impurity Hamiltonian¹¹ and point out its equivalence to the X-ray model in the infrared limit. The conserving pseudoparticle approximation up to infinite order in the hybridization V is discussed in section IV and compared with the parquet equation approach of Nozières *et al.*¹² in section V. The numerical results are discussed in section VI. In appendix A we give explicitly the self-consistent equations which determine the auxiliary particle self-energies within the CTMA.

II. PHYSICAL MODEL

The absorption of an X-ray photon by a deep level core electron and the subsequent emission of the electron leaves a core hole, which is seen by the conduction electrons as a suddenly created screened Coulomb potential. The simplest model Hamiltonian describing this situation is given by^{2,9,12-14}

$$H = \sum_{\mathbf{k}\sigma} (\epsilon_{\mathbf{k}} - \mu) c_{\mathbf{k}\sigma}^\dagger c_{\mathbf{k}\sigma} + E_d d^\dagger d + V_d \sum_{\sigma} c_{0\sigma}^\dagger c_{0\sigma} d d^\dagger, \quad (1)$$

where $c_{\mathbf{k}\sigma}$ ($c_{\mathbf{k}\sigma}^\dagger$) are the conduction electron field operators for momentum and spin eigenstates $|\mathbf{k}\sigma\rangle$, with energy $\epsilon_{\mathbf{k}}$ and chemical potential μ . The energy of the deep level is E_d , and V_d is the screened Coulomb interaction between the conduction electrons at the site of the hole ($c_{0\sigma}^\dagger$, $c_{0\sigma}$) and the hole (with operators d^\dagger , d ; the spin state of the hole is irrelevant here). We assume that the hole is localized and does not have internal structure, i.e. we neglect the finite life time of the hole due to Auger effect as well as a possible recoil of the hole. The Coulomb interaction between the conduction electrons is absorbed into a quasiparticle renormalization.

Photoemission.— The spectral function of the hole, $A_d(\epsilon)$, which can be measured in photoemission experiments, is obtained from the one-particle core hole Green's function $G_d(t) = -i\langle T[d(t)d^\dagger(0)] \rangle$, subjected to the initial condition that the core hole occupation number

$d^\dagger d = 0$ for times $t < 0$ (before the photoemission process), by taking the imaginary part of its Fourier transform, $A_d(\omega) = (1/\pi)\text{Im}G_d(\omega - i0)$. The initial condition is equivalent to the trace $\langle \dots \rangle$ in the definition of $G_d(t)$ being taken only over states with hole occupation equal to zero. It is this restriction which implies the non-trivial dynamics of the X-ray problem. $A_d(\omega)$ is proportional to the spectral weight of processes, where a photon is absorbed by the metal, subsequently emitting the deep level core electron. The energy ω required for this process is bounded from below by the threshold energy $E_0 = E_F - E_{\text{core}} - \Delta E$, where E_{core} and E_F are the core level energy and the Fermi energy, respectively, and ΔE is a renormalization due to core hole-conduction electron interactions. In the following we will choose the zero of energy such that $E_0 = 0$ (i.e. $\epsilon = \omega - E_0$). The spectral function $A_d(\epsilon)$ then shows singular threshold behavior

$$A_d(\epsilon) = \frac{C_d}{\epsilon^{\alpha_d}} \quad (\epsilon \rightarrow 0^+). \quad (2)$$

In a landmark paper Nozières and De Dominicis⁹ showed that the exponent α_d depends only on the scattering phase shift η of the conduction electrons off the core hole and calculated it as (*s*-wave-scattering)

$$\alpha_d = 1 - \left(\frac{\eta}{\pi}\right)^2 = 1 - n_d^2, \quad (3)$$

where Friedel's sum rule $\eta = \pi n_d$ has been used to express η in terms of the occupation number of the core level, n_d .

X-ray absorption.— The X-ray absorption cross section is given by the two particle Green's function $G_2(t) = -i\Theta(t)\langle [d^\dagger(t)c_{0\sigma}(t), c_{0\sigma}^\dagger(0)d(0)] \rangle$ as $d\sigma/d\epsilon \propto \text{Im}G_2(\epsilon - i0)$. The absorption cross section is finite for $\epsilon > 0$ and again shows singular threshold behavior

$$\frac{d\sigma}{d\epsilon} = \frac{C_a}{\epsilon^{\alpha_a}} \quad (\epsilon \rightarrow 0^+). \quad (4)$$

The exponent α_a has been calculated by Nozières and De Dominicis⁹ with the result

$$\alpha_a = \frac{2\eta}{\pi} - \left(\frac{\eta}{\pi}\right)^2 = 2n_d - n_d^2. \quad (5)$$

III. PSEUDOPARTICLE REPRESENTATION OF THE X-RAY MODEL

As will be seen below, it is useful to formulate the core hole problem in terms of pseudoparticles in order to impose the initial condition. We define fermion operators f^+ (f) and boson operators b^+ (b) creating (annihilating) the occupied or empty core level. The transition amplitude V of an electron from the core level into the conduction band describes the hybridization of these two systems. The Hamiltonian of this system takes the form

of an Anderson impurity Hamiltonian for spinless particles (spin degeneracy $N = 1$):

$$H = \sum_{\mathbf{k}} (\epsilon_{\mathbf{k}} - \mu) c_{\mathbf{k}}^{\dagger} c_{\mathbf{k}} + E_d f^{\dagger} f + V (f^{\dagger} b c_0 + \text{h. c.}) + \lambda Q, \quad (6)$$

where $c_0 = \sum_{\mathbf{k}} c_{\mathbf{k}}$ annihilates a conduction electron at the impurity site. The constraint $Q = f^{\dagger} f + b^{\dagger} b = 1$ ensuring that the core level is either empty or occupied is implemented by adding the last term in (6), where λ is associated with the operator constraint $Q = 1$ and may be interpreted as the negative of a chemical potential for the pseudoparticles⁴. As has been shown previously^{4,7,15}, the limit $\lambda \rightarrow \infty$ imposes the constraint exactly and is equivalent to taking all expectation values of pseudoparticle operators in the Hilbert subspace with $Q = 0$ (no core hole present). Thus, in the present context, it implements exactly the X-ray initial condition of sudden creation of the core hole. The auxiliary particle Green's functions are expressed in terms of their self-energies as $G_f^{-1}(i\omega_n) = [G_{f,b}^0(i\omega_n)]^{-1} - \Sigma_f(i\omega_n)$, $G_b^{-1}(i\nu_m) = [G_b^0(i\nu_m)]^{-1} - \Sigma_b(i\nu_m)$, where $G_f^0(i\omega_n) = 1/(i\omega_n - E_d)$ and $G_b^0(i\nu_m) = 1/i\nu_m$ are the respective non-interacting Green's functions and $i\omega_n = (2n+1)\pi/\beta$, $i\nu_m = 2m\pi/\beta$ denote the fermionic and bosonic Matsubara frequencies.

In the model (6) one may distinguish two distinct regimes, where the impurity occupation number n_d at infinitely long time after suddenly switching on the interaction is large ($n_d \rightarrow 1$, $E_d < 0$) or small ($n_d \rightarrow 0$, $E_d > 0$). Since, due to the hybridization, n_d is equal and opposite in sign to the change of the conduction electron number (i.e. screening charge) induced by the presence of the impurity, $n_d = -\Delta n_c$, these regimes correspond via the Friedel sum rule to large ($\eta \rightarrow \pi$) and small ($\eta \rightarrow 0$) scattering phase shifts, respectively (see detailed discussion below), and may, therefore, be termed the strong and the weak coupling regions. We now show the formal equivalence between the X-ray model Eq. (1) and the slave particle Hamiltonian Eq. (6) at low energies both in the weak and in the strong coupling regions.

In the strong coupling region, an effective low-energy model is derived from the Anderson Hamiltonian (6) by integrating out the slave boson degree of freedom (or, equivalently, by means of a Schrieffer-Wolff transformation¹⁶ onto the part of the Hilbert space involving only states with the core level occupied). The interaction term in the resulting effective action reads

$$S_{\text{int}} = -V^2 \frac{1}{\beta^3} \sum_{i\omega_n, i\omega'_n, i\nu_m} G_b^0(i\nu_m) \times c_0^{\dagger}(i\omega'_n - i\nu_m) c_0(i\omega_n) f(i\omega'_n) f^{\dagger}(i\omega_n + i\nu_m), \quad (7)$$

where, in addition, the projection onto the physical Hilbert space is imposed by taking $\lambda \rightarrow \infty$. At low

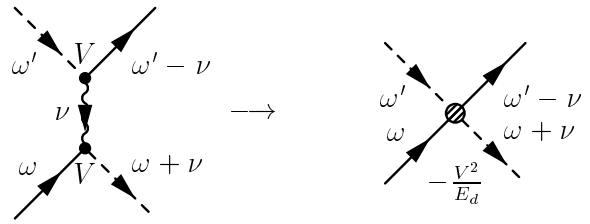


FIG. 1. Diagrammatic representation of the effective low-energy interaction in the strong coupling regime, Eq. (7), and its contraction to a density-density interaction at low excitation energies. Solid, dashed and wiggly lines correspond here and in the following to conduction electron, pseudo-fermion and slave boson propagators, respectively.

excitation energy relative to the core level, i.e. when the conduction electron energies after analytical continuation are $|\omega|, |\omega' - \nu| \ll |E_d|$ and the pseudofermions have energies $\omega', \omega + \nu \approx E_d$ (see Fig. 1), the non-interacting slave boson Green's function in Eq. (7) is taken at $\nu \approx E_d$ and thus reduces to $1/E_d$. The resulting effective Hamiltonian is thus given by Eq. (1), with electron operators d^{\dagger}, d replaced by pseudofermions f^{\dagger}, f , interacting with the conduction electrons via the repulsive, *instantaneous* potential $V_d = -V^2/E_d > 0$.

In order to derive the effective low-energy Hamiltonian in the weak coupling domain ($n_d \rightarrow 0$, $E_d > 0$), it is useful to observe that the model Eq. (6) is in the physical Hilbert space invariant under the special particle-hole transformation $f \leftrightarrow b$, $c \leftrightarrow c^{\dagger}$ and $E_d \rightarrow -E_d$. Integrating out the high energy states, i.e. the fermionic degrees of freedom in this case, and then performing this particle-hole transformation, the resulting low-energy Hamiltonian is again given by Eq. (1), with the replacement $d^{\dagger}, d \rightarrow f^{\dagger}, f$, and the attractive interaction potential $V_d = -V^2/E_d < 0$ between conduction electrons and local pseudofermions.

Having, thus, established the formal connection between the original X-ray model Eq. (1) and the auxiliary particle Hamiltonian (6) in the weak and in the strong coupling regions, we now turn to showing that the photoemission and X-ray absorption spectra are given by the slave boson and the pseudofermion spectral functions, respectively.

Photoemission.— The retarded Green's function $G_b^R(t) = -i\Theta(t)\langle [b(t), b^{\dagger}(0)]_- \rangle$ describes the propagation of the empty d -level in time. The corresponding spectral function after projection onto the physical sector $Q = 1$, $A_b^+(\omega) = -\lim_{\lambda \rightarrow \infty} \text{Im} G_b^R(\omega)/\pi$ can be represented in terms of the exact eigenstates of the system without the d -level, $|0, n\rangle$, and with the d -level, $|1, n\rangle$, as^{15,7}

$$A_b(\omega) = \frac{1}{Z_{Q=0}} \sum_{m,n} |\langle 1, m | b^{\dagger} | 0, n \rangle|^2 e^{-\beta \epsilon_{0,n}} \delta(\epsilon + \epsilon_{0,n} - \epsilon_{1,m}). \quad (8)$$

At zero temperature ($\beta = 1/T = \infty$), $A_b(\epsilon)$ is zero for $\epsilon = \omega - E_0 < 0$, where $E_0 = \epsilon_{1,0} - \epsilon_{0,0}$ is the difference

of the ground state energies for the $Q = 1$ and $Q = 0$ systems. Near the threshold, $\epsilon \gtrsim 0$, $A_b(\epsilon)$ has a power law singularity (infrared divergence), $A_b(\epsilon) \propto \epsilon^{-\alpha_b}$, for exactly the same reason as the hole spectral function $A_d(\epsilon)$ considered above: the states $|0, n\rangle$ (free Fermi sea) and $|1, n\rangle$ (Fermi sea in presence of a potential scattering center) are orthogonal, giving rise to the orthogonality catastrophe¹. The exponent α_b is therefore given in terms of the phase shift η_b (for s -wave scattering) as $\alpha_b = 1 - (\eta_b/\pi)^2$. Using the Friedel sum rule and the fact that in the photoemission process (boson propagator) the impurity occupation number changes from initially 0 to $n_d > 0$ in the final state, we obtain the characteristic dependence on n_d ,

$$\alpha_b = 1 - n_d^2. \quad (9)$$

We may conclude that the threshold behavior of the physical hole spectral function $A_d(\epsilon)$ and the slave boson spectral function $A_b(\epsilon)$ is governed by the same exponent, $\alpha_d = \alpha_b$, provided the scattering phase shift is the same.

X-ray absorption.— In a similar way, the threshold behavior of the X-ray absorption cross section $d\sigma/d\epsilon$ may be obtained from the pseudofermion Green's function. As shown in section II, $d\sigma/d\epsilon$ is proportional to the imaginary part of the two particle Green's function $G_2(t) = -i\Theta(t)\langle [d^\dagger(t)c_{0\sigma}(t), c_{0\sigma}^\dagger(0)d(0)] \rangle$. The corresponding quantity here is the slave boson-conduction electron correlation function

$$G_{bc}(t) = -i\Theta(t)\langle [b(t)c_0(t), c_{0\sigma}^\dagger(0)b^\dagger(0)] \rangle, \quad (10)$$

which is given in terms of the pseudofermion Green's function $G_f(\epsilon)$ (after Fourier transformation) as

$$G_{bc}(\epsilon) = \frac{1}{V^2} \left[(G_f^0(\epsilon))^{-1} G_f(\epsilon) - 1 \right] (G_f^0(\epsilon))^{-1}. \quad (11)$$

It follows that the spectral functions are related by $A_{bc}(\epsilon) \propto A_f(\epsilon) \sim \epsilon^{-\alpha_f}$, i.e. the X-ray absorption exponent is identical to the pseudofermion threshold exponent α_f . The latter is again determined by the orthogonality catastrophe argument, considering that the initial state of the system is now the conduction electron Fermi sea plus the filled d -level. The phase shift η_f , again given via the Friedel sum rule as the change of the occupation number from the initial to the final state, is now different, $\eta_f = (n_d - 1)\pi$, leading to the expression

$$\alpha_f = 2n_d - n_d^2. \quad (12)$$

Comparison with (5) again shows that the infrared behavior of the pseudofermion spectral function is indeed identical to that of the two particle Green's function G_2 , as expected.

It should be mentioned that in the intermediate coupling or “mixed valence” domain, $\pi N(0)V^2 \approx |E_d|$ ($n_d \approx 1/2$), a Schrieffer-Wolff type projection is no longer valid because of large level occupancy fluctuations. The formal

derivation of the X-ray model (1) from the pseudoparticle model (6) in the “mixed valence” regime involves a retarded effective interaction, in contrast to Eq. (1). However, since the Hamiltonian Eq. (6) is a faithful representation of a *non-interacting* system (via the identification $d^\dagger = f^\dagger b$), where the constraint $Q = f^\dagger f + b^\dagger b = 1$ merely serves to implement the X-ray initial condition of sudden switching on the interaction between localized states and the conduction electrons (see above), the system is described by single-particle wave functions even in the valence fluctuation regime of this spinless model. The analysis of the pseudoparticle threshold exponents α_b , α_f in terms of the corresponding scattering phase shifts η_b , η_f and the Friedel sum rule, as given above, then also applies in the valence fluctuation regime. It has been verified explicitly by a numerical renormalization group calculation of the pseudoparticle threshold exponents that their n_d dependence, given in Eqs. (9), (12), is valid over the complete range of the core level occupation number n_d ¹⁷.

The preceding analysis shows explicitly that in the auxiliary particle representation the threshold exponents of both the X-ray photoemission and absorption are determined by the infrared behavior of single-particle propagators, involving the physics of the orthogonality catastrophe for auxiliary bosons or pseudofermions only^{18,19}. *There is no separation into single particle effects and excitonic effects.*

IV. CONSERVING THEORY

In the previous section we reformulated the core hole problem by introducing auxiliary particles and showed on general grounds that the threshold exponents of X-ray absorption and photoemission spectra can be extracted from one particle properties, namely the auxiliary fermion and slave boson Green's functions respectively. In this section a systematic self-consistent approximation is formulated to calculate these functions.

As a minimal requirement the constraint $Q = 1$ has to be fulfilled in any approximate theory. The constraint is closely related to the invariance of the system under a simultaneous local (in time) gauge transformation $f(\tau) \rightarrow e^{\Theta(\tau)} f(\tau)$, $b(\tau) \rightarrow e^{\Theta(\tau)} b(\tau)$. The Lagrange multiplier λ assumes the role of a local gauge field and transforms as $\lambda \rightarrow \lambda + i\partial\Theta/\partial\tau$. Any approximate scheme respecting the gauge symmetry will preserve the charge Q in time. The simultaneous transformations $f(\tau) \rightarrow e^{\Theta(\tau)} f(\tau)$, $c_{\mathbf{k}}(\tau) \rightarrow e^{\Theta(\tau)} c_{\mathbf{k}}(\tau)$, $\mu(\tau) \rightarrow \mu(\tau) + i\partial\Theta/\partial\tau$ lead to the conservation of the total fermion number $n_f + \sum_{\mathbf{k}} c_{\mathbf{k}}^\dagger c_{\mathbf{k}} = \text{const.}$ where μ is the chemical potential of the conduction electrons (we choose $\mu = 0$). Any theory which preserves these symmetries is called conserving and may be generated by functional derivation from a generating functional Φ of closed skeleton diagrams²⁰.

NCA. — We are interested in the limit of weak hybridization V . So let us first consider the lowest order approximation. The conserving approximation scheme requires the self-energies to be determined self-consistently,

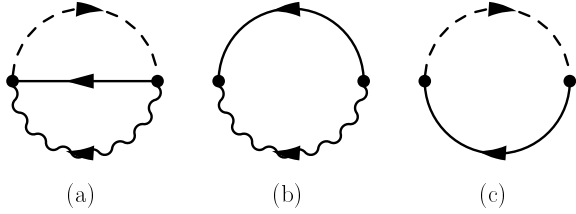


FIG. 2. (a) Diagrammatic representation of the NCA generating functional. (b) and (c) display the pseudofermion and slave boson self-energies derived from the NCA functional by functional derivation.

which amounts to an infinite resummation of perturbation theory even if only the lowest order skeleton diagram is kept (which is known as the “non-crossing approximation” (NCA)⁵, see Fig. 2). The NCA is known to yield good results in the absence of or sufficiently far away from a Fermi liquid fixed point^{21,7}. Hence the NCA is not appropriate in the X-ray problem. The reason is that no parquet diagrams (see Fig. 5) are included in the lowest order approximation. By functional derivation of Φ one obtains for the slave particle self-energies $\Sigma_f = \delta\Phi/\delta G_f$, $\Sigma_b = \delta\Phi/\delta G_b$ which are diagrammatically given in Fig. 2 and yield the set of coupled integral equations

$$\begin{aligned}\Sigma_f(\epsilon) &= V^2 \int_{-\infty}^{\infty} \frac{du}{\pi} G_b(\epsilon + u) A_c(-u) f(u) \\ \Sigma_b(\epsilon) &= V^2 \int_{-\infty}^{\infty} \frac{du}{\pi} G_f(u + \epsilon) A_c(u) f(u)\end{aligned}\quad (13)$$

where $A_c(\epsilon)$ is the non-interacting local conduction electron spectral density. At zero temperature $T = 0$ the integral equations can be rewritten as ordinary differential equations (with a constant density of states for the conduction electrons and for $\epsilon \rightarrow 0$)²²

$$\frac{\partial}{\partial \epsilon} \frac{1}{A_f(\epsilon)} \sim N(0)V^2 A_b(\epsilon)$$

$$\frac{\partial}{\partial \epsilon} \frac{1}{A_b(\epsilon)} \sim N(0)V^2 A_f(\epsilon). \quad (14)$$

The solution displays the well-known infrared singularities $A_{f,b}(\epsilon) \propto \epsilon^{-\alpha_{f,b}}$ ($\epsilon \rightarrow 0$) where $\alpha_{f,b} = 1/2$. These exponents obviously differ from the exact results discussed before [Eqs. (9) and (12)].

Hence the NCA is not even in qualitative agreement with the exact Fermi liquid properties of the model; it shows no dependence of the exponents on the filling factor n_d of the deep level. This is due to the lack of vertex corrections which have to be included in infinite orders of perturbation theory, because it can be shown by power-counting arguments that there are no corrections to the NCA exponents in any finite order²¹.

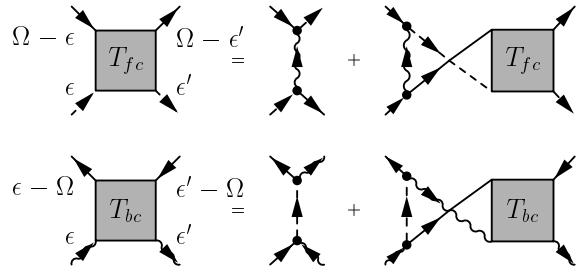


FIG. 3. Diagrammatic representation of the Bethe-Salpeter equations for the T -matrices in Eqs. (15) and (16), respectively. The analytically continued equations, which are calculated numerically, are discussed in appendix A.

CTMA. — We have to include the major singularities in each order of self-consistent perturbation theory. These singularities emerge in the conduction electron and pseudofermion T -matrix (T_{fc}) as well as in the conduction electron and slave boson T -matrix (T_{bc}). In order to preserve gauge invariance, self-consistency has to be imposed: the self-energies are functionals of the Green’s functions which in turn are expressed in terms of self-energies, closing the set of self-consistent equations. The summation of the corresponding ladder diagrams can be performed by solving the integral equations for the T -matrices for the pseudofermions (see Fig. 3)⁶

$$\begin{aligned}T_{fc}(i\omega_n, i\omega'_n; i\Omega_m) &= V^2 G_b(i\omega_n + i\omega'_n - i\Omega_m) \\ &\quad - \frac{V^2}{\beta} \sum_{i\omega''_n} G_b(i\omega_n + i\omega''_n - i\Omega_m) G_f(i\omega''_n) G_c(i\Omega_m - i\omega''_n) T_{fc}(i\omega''_n, i\omega'_n; i\Omega_m),\end{aligned}\quad (15)$$

and the slave-bosons

$$\begin{aligned}T_{bc}(i\nu_m, i\nu'_m; i\Omega_n) &= V^2 G_f(i\nu_m + i\nu'_m - i\Omega_n) \\ &\quad - \frac{V^2}{\beta} \sum_{i\nu''_m} G_f(i\nu_m + i\nu''_m - i\Omega_n) G_b(i\nu''_m) G_c(-i\Omega_n - i\nu''_m) T_{bc}(i\nu''_m, i\nu'_m; i\Omega_n).\end{aligned}\quad (16)$$

Here $\omega_n, \omega'_n, \omega''_n$ are fermionic frequencies ($\omega_n = (2n + 1)\pi/\beta$), ν_m, ν'_m, ν''_m are bosonic frequencies ($\nu_m = 2m\pi/\beta$), and the center of mass frequency $\Omega_{m,n}$ is bosonic in the case of T_{fc} and fermionic for T_{bc} . The self-energies Σ_f and Σ_b

$$\Sigma_f(i\omega_n) = \Sigma_f^{\text{NCA}}(i\omega_n) + \Sigma_f^{fc}(i\omega_n) + \Sigma_f^{bc}(i\omega_n) \quad (17)$$

$$\Sigma_b(i\nu_m) = \Sigma_b^{\text{NCA}}(i\nu_m) + \Sigma_b^{fc}(i\nu_m) + \Sigma_b^{bc}(i\nu_m) \quad (18)$$

calculated from T_{fc} and T_{bc} , then follow from a generating functional Φ (see Fig. 4) by functional derivation. The explicit expressions are given in appendix A.

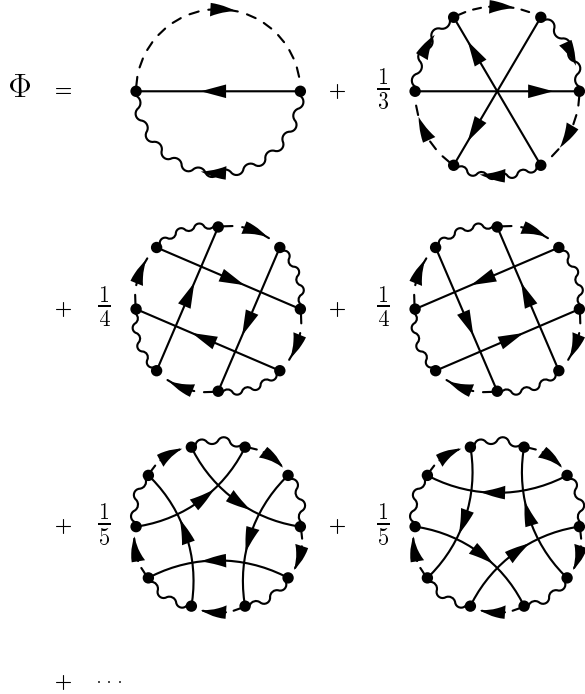


FIG. 4. Diagrammatic representation of the CTMA generating functional. The free energy diagram with two conduction electron lines does not appear, since it is not a skeleton diagram.

V. COMPARISON WITH RENORMALIZED PARQUET EQUATIONS

The CTMA is closely related to the parquet equation approach by Nozières *et al.* In Ref. [14] these authors investigate the X-ray model (1) by the methods of perturbation theory. Even to the lowest order one must sum the so-called parquet diagrams, in close analogy with the Abrikosov theory of the Kondo effect²³. In this approximation Mahan's prediction² of the singularity in the X-ray absorption spectrum was first confirmed. In a succeeding paper¹² the many-body approach was generalized to include self-energy and vertex renormalization in a self-consistent fashion. This self-consistent formalism

describes the reaction of divergent fluctuations on themselves, and should, therefore, be useful in other more complicated problems, such as the Kondo effect.

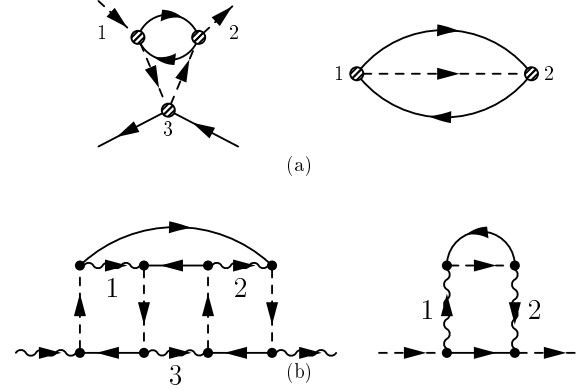


FIG. 5. (a) Vertex renormalization and self-energy reproduced from the parquet equation approach¹². These diagrams are obtained from the corresponding ones in (b) by contracting the boson-lines 1, 2 and 3. The CTMA, therefore, contains the parquet contributions of Ref. [12] as a diagrammatic subclass.

In Ref. [12] it is shown that the significant contributions in logarithmic accuracy to the renormalized interaction and the deep level self-energy are given by the diagrams reproduced in Fig. 5 (a). Both graphs are included in the CTMA (see Fig. 5 (b)): By collapsing the boson lines into points, i.e. by integrating out the high energy bosonic degree of freedom in the strong coupling region ($n_d \rightarrow 1$) as done in section III, it is seen that the X-ray interaction kernel (Fig. 5 (a), left) can be extracted from the T_{bc} -matrix, and the deep level self-energy (Fig. 5 (a), right) is already included in the NCA. For weak coupling ($n_d \rightarrow 0$) analogous results are obtained by integrating out the pseudofermionic degree of freedom and then interchanging bosons and fermions, compare section III. The *self-consistent* evaluation of these diagrams represents the renormalized parquet analysis for the pseudoparticles. *The advantage of our formulation is that it is valid both in the weak coupling and in the strong coupling regime, with symmetrical expressions in these two regions.* The symmetry between weak and strong coupling is also visible in the results for the threshold exponents (Fig. 7). Since the CTMA is not restricted to parquet diagrams (which give the right asymptotic behaviour only for $V \rightarrow 0$), but goes beyond the parquet approximation, one may expect that its validity extends beyond the weak and the strong coupling limits and interpolates correctly between these regimes. This will be seen the following section.

VI. NUMERICAL RESULTS

The self-consistent solutions are obtained by first solving the linear Bethe-Salpeter equations (11) and (12) for the T -matrices by matrix inversion on a grid of 200 frequency points. First we insert NCA Green's functions into the T -matrix equations. From the T -matrices the auxiliary particle self-energies Σ_f and Σ_b are calculated corresponding to Eqs. (7) and (10), which give the respective Green's functions. This process is iterated until

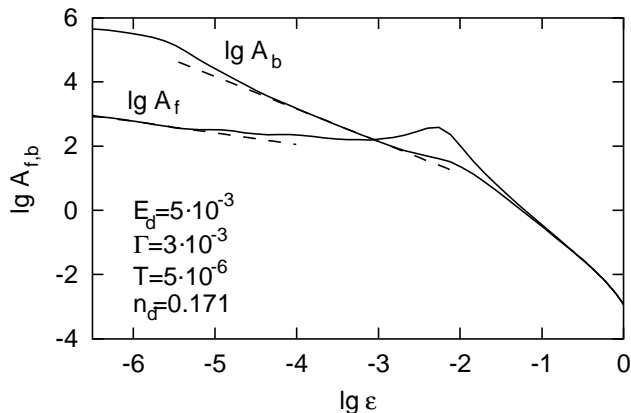


FIG. 6. Auxiliary particle spectral functions A_f and A_b in the weak coupling regime in a logarithmic plot. The energies are in units of the half band width D . The slopes of the dashed lines indicate the exact threshold exponents.

convergence is reached²⁴. The T -matrices show nonanalytic behavior in the infrared limit.

As can be seen from Fig. 6 the fermion and boson spectral functions display power law behaviour at low frequencies²⁵. The power law behaviour emerges in the infrared limit, i.e. for energies smaller than the low energy scale (which is E_d). For smaller frequencies there is always a deviation from the power law behaviour due to finite temperature. The exponents extracted from the spectral functions at low but finite temperature for various values of the deep level filling n_d in Fig. 7 are in good numerical agreement with the exact results in the regions $n_d \in [0.0, 0.3]$ and $n_d \in [0.7, 1.0]$. Note that in contrast to the n_d -dependent exponents within the CTMA the NCA spectral functions always diverge with n_d -independent exponents $\alpha_f = \alpha_b = 1/2$. For intermediate coupling, $n_d \in [0.3, 0.7]$, the convergence of the self-consistent scheme is very slow, and we find no stable numerical solution. It remains to be seen whether this is due to numerical instabilities or possibly due to the importance of further vertex corrections beyond the CTMA.

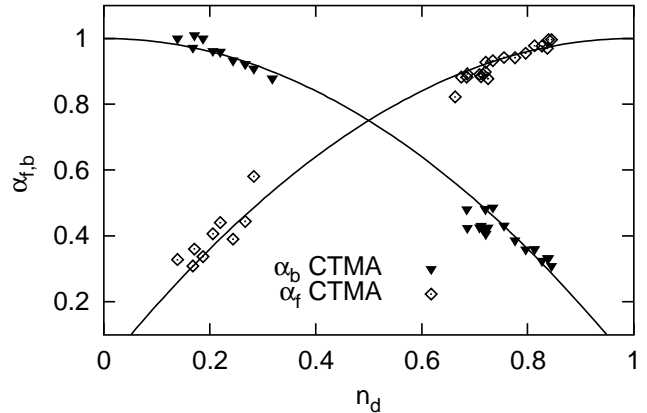


FIG. 7. Auxiliary particle threshold exponents extracted from spectra as in Fig. 8 for a number of deep level fillings n_d . The solid lines represent the exact values derived in Eqs. (9) and (12).

A comparison of the CTMA results with the weak-coupling treatment, which corresponds to $n_d \rightarrow 0$ in our model, shows that for finite interaction strength renormalization effects are important (see Fig. 8). The connection between n_d and E_d/Γ is exactly given by Friedel's sum rule $n_d = 1/2 - \arctan(E_d/\Gamma)/\pi$. Again we mention the n_d dependence of the exponent α_f in contrast to the NCA result: To recover the Fermi liquid properties of the model one thus has to go far beyond the lowest order self-consistent approximation.

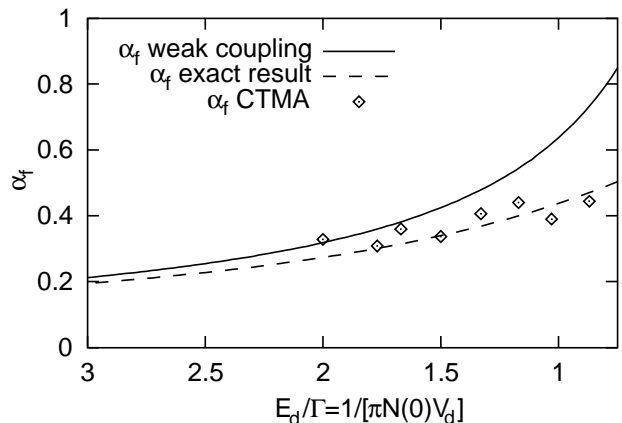


FIG. 8. Comparison of the CTMA results and the weak-coupling calculation^{12,14} for the threshold exponent of X-ray absorption spectra.

VII. CONCLUSION

In summary, we have calculated the exponents of threshold singularities in the X-ray photoemission and

absorption spectra, using a standard many-body technique, where the empty and the singly occupied core level are represented by separate fields, auxiliary bosons and pseudofermions, respectively, coupled to the conduction electrons via a hybridization interaction. In this formulation, the X-ray problem is described by a spinless Anderson impurity model in pseudoparticle representation, and the initial condition of sudden creation of the impurity potential is implemented by the constraint that all expectation values of local fermion or boson fields must be calculated in the Hilbert subspace with pseudoparticle number $Q = 0$. The latter can be fulfilled exactly. It was further shown that the X-ray photoemission cross section or core level spectral function is given by the boson spectral function, while the X-ray absorption cross section is proportional to the total fermion hybridization vertex. Therefore, the X-ray photoemission and absorption threshold exponents are identical to the infrared exponents of the auxiliary boson and pseudofermion spectral functions, respectively. It follows that both X-ray photoemission and absorption are solely governed by the orthogonality catastrophe, and there is no separation into single particle and excitonic effects.

In a more general context, the generalized $SU(N) \times SU(M)$ Anderson impurity models, classified by the spin degeneracy N of the local orbital and the number M of degenerate conduction electron channels, may be considered as standard models to describe strong correlations induced by the restriction of no double occupancy of sites. Depending on their symmetry, these models display Fermi ($N = M = 1$ or $N \geq M + 1$) or non-Fermi liquid behavior ($2 \leq N \leq M$) at low temperature²¹. The present case of the spinless Anderson impurity model in slave boson representation ($N = 1, M = 1$), Eq. (6), may be considered as the most stringent test case for the development of new methods for strongly correlated systems. This is because for this case earlier approximation schemes like the non-crossing approximation (NCA) fail in the most pronounced way to even qualitatively describe the low-energy Fermi liquid behavior of this

model, i.e. the n_d dependence of the infrared threshold exponents, while in the non-Fermi liquid case the NCA gives the correct exponents at least in the Kondo limit of these models²¹.

In the present paper we have applied a recently developed approximation scheme, the conserving T -matrix approximation (CTMA) to the $N = 1, M = 1$ Anderson impurity model to calculate the X-ray photoemission and absorption threshold exponents on a common footing. The CTMA includes the complete subclass of diagrammatic contributions which, in the limits of weak ($n_d \rightarrow 0$) and strong ($n_d \rightarrow 1$) impurity scattering potential, reduce to the renormalized parquet diagrams, which have been shown by Nozières et al.¹² to describe the exact infrared singular behavior in the weak coupling regime of the X-ray problem. As a result, the CTMA recovers the correct X-ray photoemission and absorption exponents in a wide region around weak as well as strong coupling. In connection with earlier results⁶ on the spin 1/2 Anderson impurity model ($N = 2, M = 1$), this makes the CTMA the first standard many-body technique to correctly describe the Fermi liquid regime of the Anderson impurity models in a systematic way, including the smooth crossover to the high temperature behavior.

We are grateful for discussions with J. Brinkmann, T. A. Costi and T. Kopp. T.S. acknowledges the support of the DFG-Graduiertenkolleg "Kollektive Phänomene im Festkörper". This work was supported in part by SFB 195 of the Deutsche Forschungsgemeinschaft. Computer support was provided by the John-von-Neumann Institute for Computing, Jülich.

APPENDIX A: CTMA EQUATIONS

In this appendix we give explicitly the self-consistent equations which determine the auxiliary particle self-energies within the CTMA. In the Matsubara representation the vertex functions T_{fc} and T_{bc} are given by the following Bethe-Salpeter equations:

$$T_{fc}(i\omega_n, i\omega'_n; i\Omega_m) = I_{fc}(i\omega_n, i\omega'_n; i\Omega_m) + \frac{V^2}{\beta} \sum_{i\omega''_n} G_b(i\omega_n + i\omega''_n - i\Omega_m) G_f(i\omega''_n) G_c(i\Omega_m - i\omega''_n) T_{fc}(i\omega''_n, i\omega'_n; i\Omega_m) \quad (1)$$

with

$$I_{fc}(i\omega_n, i\omega'_n; i\Omega_m) = -\frac{V^4}{\beta} \sum_{i\omega''_n} G_b(i\omega_n + i\omega''_n - i\Omega_m) G_f(i\omega''_n) G_c(i\Omega_m - i\omega''_n) G_b(i\omega'_n + i\omega''_n - i\Omega_m),$$

and T_{bc}

$$T_{bc}(i\nu_m, i\nu'_m; i\Omega_n) = I_{bc}(i\nu_m, i\nu'_m; i\Omega_n) - \frac{V^2}{\beta} \sum_{i\nu''_m} G_f(i\nu_m + i\nu''_m - i\Omega_n) G_b(i\nu''_m) G_c(i\nu''_m - i\Omega_n) T_{bc}(i\nu''_m, i\nu'_m; i\Omega_n) \quad (2)$$

with

$$I_{bc}(i\nu_m, i\nu'_m; i\Omega_n) = -\frac{V^4}{\beta} \sum_{i\nu''_m} G_f(i\nu_m + i\nu''_m - i\Omega_n) G_b(i\nu''_m) G_c(i\nu''_m - i\Omega_n) G_f(i\nu'_m + i\nu''_m - i\Omega_n).$$

Note that, in addition to the different sign in T_{fc} , these vertex functions differ from the T -matrices defined before in that they contain only terms with two or more rungs, since the inhomogenous parts I_{fc} and I_{bc} represent terms

with two bosonic or fermionic rungs, respectively. The terms with a single rung correspond to the NCA diagrams and are evaluated separately.

The fermion self-energies in Fig. 9 are given by

$$\Sigma_f^{fc}(i\omega_n) = \frac{1}{\beta} \sum_{i\Omega_m - i\omega_n} G_c(i\Omega_m - i\omega_n) T_{fc}(i\omega_n, i\omega_n; i\Omega_m) \quad (3)$$

$$\Sigma_f^{bc}(i\omega_n) = -\frac{V^2}{\beta^2} \sum_{i\nu'_m, i\nu''_m} G_c(i\omega_n - i\nu'_m) G_b(i\nu'_m) G_c(i\omega_n - i\nu''_m) G_b(i\nu''_m) T_{bc}(i\nu'_m, i\nu''_m; i\nu'_m + i\nu''_m - i\omega_n) \quad (4)$$

and the boson self-energies by

$$\Sigma_b^{bc}(i\nu_m) = \frac{1}{\beta} \sum_{i\nu_m - i\Omega_n} G_c(i\nu_m - i\Omega_n) T_{bc}(i\nu_m, i\nu_m; i\Omega_n) \quad (5)$$

$$\Sigma_b^{fc}(i\omega_n) = -\frac{V^2}{\beta^2} \sum_{i\omega'_n, i\omega''_n} G_c(i\omega'_n - i\nu'_m) G_f(i\omega'_n) G_c(i\omega''_n - i\nu_m) G_f(i\omega''_n) T_{fc}(i\omega'_n, i\omega''_n; i\omega'_n + i\omega''_n - i\nu_m). \quad (6)$$

After analytical continuation to the real frequency axis we have to solve the NCA equations (13) and the following CTMA equations

$$\Sigma_f^{fc}(\epsilon) = \int_{-\infty}^{\infty} \frac{du}{\pi} f(u - \epsilon) A_c(u - \epsilon) T_{fc}(\epsilon, \epsilon; u) \quad (7)$$

$$\Sigma_f^{bc}(\epsilon) = -V^2 \int_{-\infty}^{\infty} \frac{du}{\pi} \int_{-\infty}^{\infty} \frac{du'}{\pi} f(u - \epsilon) f(u' - \epsilon) A_c(\epsilon - u') G_b(\epsilon) T_{bc}(u, u'; u + u' - \epsilon) A_c(\epsilon - u') G_b(u') \quad (8)$$

$$\Sigma_b^{bc}(\epsilon) = -\int_{-\infty}^{\infty} \frac{du}{\pi} f(u - \epsilon) A_c(\epsilon - u) T_{bc}(\epsilon, \epsilon; u) \quad (9)$$

$$\Sigma_b^{fc}(\epsilon) = -V^2 \int_{-\infty}^{\infty} \frac{du}{\pi} \int_{-\infty}^{\infty} \frac{du'}{\pi} f(u - \epsilon) f(u' - \epsilon) A_c(\epsilon - u) G_f(\epsilon) T_{fc}(u, u'; u + u' - \epsilon) A_c(u' - \epsilon) G_f(u') \quad (10)$$

with the fermion-conduction electron vertex function

$$T_{fc}(\epsilon, \epsilon'; \Omega) = I_{fc}(\epsilon, \epsilon'; \Omega) - V^2 \int_{-\infty}^{\infty} \frac{du}{\pi} f(u - \Omega) G_b(\epsilon + u - \Omega) G_f(u) A_c(\Omega - u) T_{fc}(u, \epsilon'; \Omega) \quad (11)$$

$$I_{fc}(\epsilon, \epsilon'; \Omega) = V^4 \int_{-\infty}^{\infty} \frac{du}{\pi} f(u - \Omega) G_b(\epsilon + u - \Omega) G_f(u) A_c(\Omega - u) G_b(\epsilon' + u - \Omega)$$

and the boson-conduction electron vertex function

$$T_{bc}(\epsilon, \epsilon'; \Omega) = I_{bc}(\epsilon, \epsilon'; \Omega) - V^2 \int_{-\infty}^{\infty} \frac{du}{\pi} f(u - \Omega) G_f(\epsilon + u - \Omega) G_b(u) A_c(u - \Omega) T_{bc}(u, \epsilon'; \Omega) \quad (12)$$

$$I_{bc}(\epsilon, \epsilon'; \Omega) = -V^4 \int_{-\infty}^{\infty} \frac{du}{\pi} f(u - \Omega) G_f(\epsilon + u - \Omega) G_b(x) A_c(u - \Omega) G_f(\epsilon' + u - \Omega).$$

Note that the self-energy contributions obtained from the two rung T -matrix terms (I_{fc} and I_{bc}) display no skeleton diagrams; they are subtracted in the end.

$$\Sigma_b = \text{[diagram 1]} + T_{bc} + \text{[diagram 2]}$$

$$\Sigma_f = \text{[diagram 3]} + T_{fc} + \text{[diagram 4]}$$

FIG. 9. Diagrammatic representation of the NCA and CTMA expressions for the pseudoparticle self-energies.

-
- ¹ P. W. Anderson, Phys. Rev. Lett. **18**, 1049 (1967); Phys. Rev. **164**, 352 (1967).
² G. D. Mahan, Phys. Rev. **153**, 882 (1967); Phys. Rev. **163**, 612 (1967).
³ S. E. Barnes, J. Phys. F. **6**, 1375 (1976); **7**, 2637 (1977).
⁴ P. Coleman, Phys. Rev. B **29**, 3035 (1984).
⁵ H. Keiter and J. C. Kimball, J. Appl. Phys. **42**, 1460 (1971); N. Grewe and H. Keiter, Phys. Rev. B **24**, 4420 (1981); Y. Kuramoto, Z. Phys. B **53**, 37 (1983).
⁶ J. Kroha, P. Wölfle and T. A. Costi, Phys. Rev. Lett. **79**, 261 (1997).
⁷ J. Kroha and P. Wölfle, Acta Physica Polonica B **29**, 3781 (1998).

- ⁸ S. Böcker, J. Kroha, and P. Wölfle (unpublished).
⁹ P. Nozières and C. T. De Dominicis, Phys. Rev. **178**, 1097 (1969).
¹⁰ K. D. Schotte and U. Schotte, Phys. Rev. **182**, 479 (1969).
¹¹ B. Menge and E. Müller-Hartmann, Z. Phys. B **73**, 225 (1988).
¹² P. Nozières, J. Gavoret, and B. Roulet, Phys. Rev. **178**, 1084 (1969).
¹³ For an overview see: K. Ohtaka and Y. Tanabe, Rev. Mod. Phys. **62**, 929 (1990) and references therein.
¹⁴ B. Roulet, J. Gavoret, and P. Nozières, Phys. Rev. **178**, 1072 (1969).
¹⁵ T. A. Costi, J. Kroha, and P. Wölfle, Phys. Rev. B **53**, 1850 (1995).
¹⁶ J. R. Schrieffer and P. A. Wolff, Phys. Rev. **149**, 491 (1966).
¹⁷ T. A. Costi, P. Schmitteckert, J. Kroha, and P. Wölfle, Physica C **235-240**,
¹⁸ J. J. Hopfield, Comments Solid State Phys. **2**, 40 (1969).
¹⁹ K. D. Schotte and U. Schotte, Phys. Rev. B **185**, 509 (1969).
²⁰ G. Baym, and L. P. Kadanoff, Phys. Rev. **124**, 287 (1961); G. Baym, Phys. Rev. **127**, 1391 (1962).
²¹ D. L. Cox and A. E. Ruckenstein, Phys. Rev. Lett **71**, 1613 (1993).
²² E. Müller-Hartmann, Z. Phys. B **57**, 281 (1984).
²³ A. A. Abrikosov, Physics **2**, 5 (1965).
²⁴ The criterion of convergence is defined as follows. If the relative change of two successive iterations is smaller than $5.0 \cdot 10^{-3}$ the solution is assumed to be converged.
²⁵ In the numerical calculations we choose small values for E_d and Γ of $\mathcal{O}(10^{-3})$. The reason is that the solution of the self-consistent equations is not stable for E_d values of the order of the half bandwidth D ; this may be due to influence of the high energy cut-off.